Neutron investigation of the dynamical properties of the mercury-chain compound $Hg_{3-\delta}$ AsF_6

I. U. Heilmann, J. D. Axe, J. M. Hastings, and G. Shirane
Brookhaven National Laboratory, Upton, New York 11973

A. J. Heeger* and A. G. MacDiarmid†
Laboratory for Research on the Structure of Matter, University of Pennsylvania, Philadelphia, Pennsylvania 19104
(Received 26 February 1979)

We present in this paper the results of a detailed neutron scattering investigation at various temperatures of the dynamical properties of the linear-mercury-chain compound $Hg_{3-\delta}$ AsF_6. The main emphasis has been put on the nature of the response function of the Hg chains at higher temperatures ($T \gtrsim 150$ K). The results are analyzed and discussed in terms of new theoretical results obtained by Emery and Axe, and it is found that the behavior of the Hg chains in this temperature region is one-dimensional liquidlike, in accordance with theoretical predictions. Below $T_c = 120$ K where three-dimensional long-range order is established among the Hg ions, the transverse phononlike excitations in the Hg chains with displacement along the chain develop a small (~ 0.1 meV) energy gap at finite wave vector. This feature makes it straightforward to demonstrate the absence of elastic scattering in the sheets of scattering from the Hg chains. We have measured at room temperature acoustic AsF_6 sublattice phonons in the $\Delta(\zeta 00)$ and the $\Lambda(00\zeta)$ directions. The observed dispersion slope of the transverse branch along Δ polarized along Λ is about 25% smaller than that of the transverse branch along Λ polarized along Δ, in apparent disagreement with elasticity theory which predicts both modes to be governed by C_{44}. We show that this behavior can be qualitatively explained by the anisotropic coupling between Hg chains and the host lattice, leading to a much smaller elastic regime in the Λ direction than in the Δ direction.

I. INTRODUCTION

As a result of its anisotropic linear-chain arrangement of mercury ions and its incommensurability, the compound $Hg_{3-\delta}$ AsF_6 displays a number of interesting physical properties, as unveiled in several experimental studies recently.[1-6] In contrast to the incommensurability of a small displacement wave relative to the underlying lattice observed in, e.g., certain one-dimensional conductors [such as tetrathiafulvalenium-tetracyanoquinodimethanide (TTF-TCNQ)][7], $Hg_{3-\delta}$ AsF_6 features a truly structural incommensurability. As reflected in the nonstoichiometric formula ($\delta \simeq 0.18$ at $T = 300$ K) the Hg-Hg distance along the chains is incommensurate with the lattice constant a_L of the host lattice of AsF_6^- groups, in which the Hg chains are accommodated. This property implies that—apart from constraining the Hg chain positions to an ordered array—the interaction between the Hg chains and the host lattice is negligible.[8,9]

Figure 1(a) shows schematically the arrangement of the Hg chains within the tetragonal unit cell of the host lattice as determined by means of x-ray diffraction[1] and neutron diffraction.[2] There are two orthogonal and nonintersecting arrays of Hg chains parallel to the tetragonal a_L and b_L axes, respectively, and thus no Hg chains in the c_L direction. At room temperature, it was shown by x-ray and neutron scattering studies[1,3] that, apart

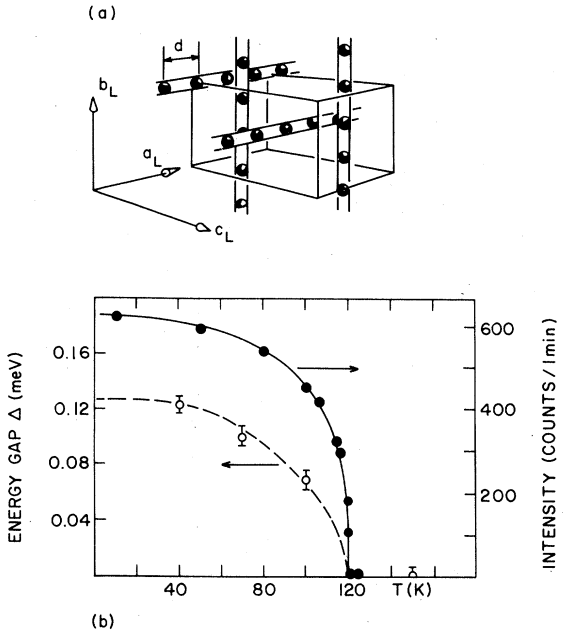

FIG. 1. (a) Spatial arrangement of Hg chains within the tetragonal unit cell of AsF_6 groups. The crystal orientation shown is that of the experiments, i.e., with a (hOl) zone in the scattering (horizontal) plane. (b) Temperature dependence of the intensity of the Bragg peak at $(3-\delta, 1-\delta, 0)$ (filled circles) and the energy gap in the dispersion of phonon-like excitations in the Hg chains (open circles), showing the phase transition at $T_c = 120$ K.

from Bragg peaks at $(0kl)$, the array of chains along a_L gives rise to diffuse scattering uniformly distributed in thin sheets $[n(3-\delta), k, l]$. Scattering distributed in an analogous manner is produced by the other array of Hg chains. These observations imply; (i) that there is a large correlation length within each chain, (ii) there is virtually no correlation between Hg ions belonging to different chains, and (iii) that the nearest-neighbor intrachain Hg-Hg distance d as determined by $2\pi/d = (3-\delta)a_L^*$ leading to the incommensurate value $d = a_L/(3-\delta)$. This shows that at higher temperatures ($T \gtrsim 300$ K) the coupling between different Hg chains is unimportant and the chains behave like truly one-dimensional entities.

By lowering the temperature an increasing modulation of the scattering in the (first) sheet was observed, arising from a growing correlation between Hg ions in different parallel chains.[3,10] Below $T = 125$ K this short-range order modulation falls abruptly, and is replaced by the development of Bragg peaks below $T_c = 120$ K. The temperature dependence of the observed Bragg intensity at $\vec{Q} = (3-\delta, 1-\delta, 0)$ is shown by the filled circles in Fig. 1b. Below $T_c = 120$ K each of the two orthogonal arrays of Hg chains build up body-centered monoclinic sublattices sharing common reciprocal lattice points, indicating that the phase transition at $T_c = 120$ K is governed by interaction between perpendicular chains.

In addition to the regular acoustic lattice phonons, Hastings *et al.*[3] measured at room temperature excitations which reliably could be assigned to "one-dimensional" phonon modes in the individual Hg chains. The situation is visualized in Fig. 2. The scattering plane is the $a_L^* c_L^*$ plane of reciprocal space and thus contains one of the two orthogonal chain directions (along a_L^*). Idealized dispersion curves in the a_L^* direction are shown for regular acoustic lattice phonons (with a period of $2a_L^*$, due to the body-centered lattice) and for longitudinal phonons associated with the Hg chains [with a period of $(3-\delta)\, a_L^*$, incommensurate with a_L^*]. Portions of the dispersion surfaces in the $a_L^* c_L^*$ plane are likewise shown. Hastings *et al.*[3] measured the Hg chain phonon dispersion along a_L^* for energies between 2 and 5 meV and found in this range a virtually linear dispersion relation with a slope of $4.4\ (0.8) \times 10^5$ cm/sec, almost twice as large as the initial slope of the acoustic lattice phonons. Moreover, these authors found the dispersion relation to depend solely on the component Q_{a^*} along the chain direction of the momentum transfer $\vec{Q}$, thus demonstrating the one-dimensional character of the excitations.

Recently, inelastic neutron measurements of the Hg chain excitations were carried out at several

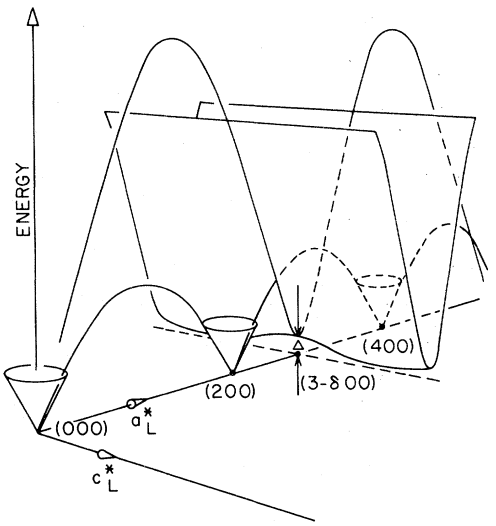

FIG. 2. Idealized dispersion relations in the $a_L^* c_L^*$ reciprocal plane. Along the a_L^* direction (chain direction) is shown dispersion curves for acoustic lattice phonons (period $2a_L^*$) as well as for phononlike excitations in the Hg-chains [period $(3-\delta)\ a_L^*$]. Portions of the dispersion surfaces are likewise shown. Note that $(3-\delta, 0, 0)$ is not a reciprocal lattice point of the Hg sublattice at low temperatures.

temperatures below T_c,[11] demonstrating the presence of an energy gap Δ in the Hg chain dispersion at the point $\vec{Q} = (3-\delta, 0, 0)$ as indicated in Fig. 2. The temperature dependence of Δ thus found is shown in Fig. 1b (open circles) and indicates that the presence of Δ is caused by the chain-chain interaction. Furthermore, it could be readily demonstrated that the scattering in the sheets for temperatures below T_c is entirely inelastic, suggesting that this is the case above T_c as well. The verification of the latter point is a crucial test of the recent theoretical prediction of Emery and Axe,[8] that in the high-temperature limit the response from the Hg chains is that of a one-dimensional liquid.

The remaining part of the present article is organized in the following manner. In Sec. II we present briefly the basic assumptions and the main results of the theoretical model of Emery and Axe, relevant for the interpretation of the measurements presented here. Section III describes experimental details. Quasielastic measurements of the diffuse sheets were carried out for a range of T and Q values, and the analysis of these measurements in terms of the theoretically predicted results (Sec. II) is presented in Sec. IV A. Inelastic measurements were carried out at the first sheet, probing the Hg chain excitations. The results obtained at room temperature are pre-

sented in Sec. IV B and are analyzed by means of the model cross section. The inelastic measurements carried out at lower temperatures are presented and discussed in Sec. IV C. In Sec. IV D we present room-temperature measurements of the dispersions of acoustic, transverse lattice modes propagating along a_L and c_L, showing an apparent disagreement with elasticity requirements. A qualitative explanation of the observations is given. Finally, Sec. V contains a summary and concluding remarks.

II. THEORY

In the model of Emery and Axe[8] the Hamiltonian H for the total system of Hg chains is written as a sum of one-dimensional Hamiltonians H^0 for the individual chains and terms describing the interchain coupling within each of the two orthogonal arrays and the coupling between perpendicular chains, respectively. Within a particular chain only nearest-neighbor coupling is considered and is assumed harmonic in the relative deviation from the equilibrium separation d. Thus

$$H^0 = \frac{1}{2}\sum_{\alpha}\frac{\pi_\alpha^2}{m} + \frac{mv^2}{d^2}(x_{\alpha+1} - x_\alpha - d)^2 , \qquad (1)$$

where x_α, and π_α are the position and momentum (along the chain) of the αth Hg ion, respectively, and m is the Hg mass. The force constant is expressed in terms of the longitudinal sound velocity v of the chain. The coupled chain problem is treated using a generalized mean-field approximation, which is able to explain successfully the short-range order modulation of the first sheet as well as the details of the phase-ordering phase transition at $T_c = 120$ K.

Below T_c ion charge-density waves along the chains are developed, first with wave vector $2\pi/d$ and then gradually higher harmonics $n2\pi/d$, whose amplitudes at low temperatures saturate, thus describing a fully developed sublattice of Hg ions. This predicted behavior is analogous to mean-field theoretical results for the nematic-to-smectic-A transition in liquid crystals, obtained by Meyer and Lubensky.[12] In this case, a set of order parameters are the Fourier components of the density in the direction perpendicular to the smectic planes, and it was recently established by x-ray technique,[13] that just below T_c only the first harmonic is present.

In the present work we are mainly concerned about the properties of the system at temperatures well above T_c. In this region the effect of the coupling terms is negligible and consequently the scattering is essentially that of the separate chains. We therefore concentrate on the response function corresponding to the Hamiltonian H^0, Eq. (1), of the individual chain. It has been shown[8] that the Fourier transform of the pair correlation function of this system is given by

$$S^0(Q) = \sinh(\tfrac{1}{2}\sigma^2Q^2)/[\cosh(\tfrac{1}{2}\sigma^2Q^2) - \cos Qd] , \qquad (2)$$

where $\sigma^2 = d^2kT/mv^2$ is the mean-square deviation in the distance of nearest-neighbor Hg ions and Q is the momentum along the chain. One notes that the scattering function Eq. (2) is structureless for large values of Q, $S^0(Q) \to 1$ for $Q \to \infty$. This reflects the fact that the one-dimensional chain has no long-range order (for $T > 0$). For smaller Q's, the scattering function Eq. (2) displays a series of peaks at $Q_n = n\,2\pi/d$, which in the limit $Qd \gg \sigma^2/d^2$ are nearly Lorentzian with a half width at half maximum equal to

$$\kappa_n = 2\pi^2(\sigma/d)^2\,(n^2/d) = 2\pi^2(kT/mv^2d)n^2 . \qquad (3)$$

Thus, the series of planes of diffuse scattering predicted by the one-dimensional independent-chain Hamiltonian Eq. (1) has half widths proportional to the temperature T and proportional to the square of the order n of the sheets. One notes furthermore that Eq. (3) does not contain any adjustable parameter since v and d are directly determined by experiment.

The dynamical properties of the model in the independent-chain limit yields a calculation of the time-dependent pair correlation function corresponding to the Hamiltonian Eq. (1). The result in the vicinity of the nth sheet (i.e., $|q_n| \equiv |Q - Q_n| \ll d^{-1}$) is

$$S^0(Q,\omega) = \frac{4}{\pi dv}\,\frac{\kappa_n}{(q_n + \omega/v)^2 + \kappa_n^2}\,\frac{\kappa_n}{(q_n - \omega/v)^2 + \kappa_n^2} . \qquad (4)$$

It can be verified that the result Eq. (2) is recovered by performing the integration $\int S^0(Q,\omega)\,d\omega$. The expression in Eq. (4) is the full density-density correlation function for the system and it is instructive to compare it to the scattering function resulting from a conventional multiphonon expansion applied to a (hypothetical ordered) linear, monatomic chain. As is well known in the latter case, at relatively low temperature and momentum transfer, the major part of the coherent scattering is the elastic (Bragg) scattering and the inelastic one-phonon scattering. Within the harmonic approximation the elastic cross section consists of δ functions at the Bragg points $Q_n = n2\pi/d$, with relative intensities governed by the usual Debye-Waller factor e^{-2W}. Likewise, the one-phonon cross section consists of δ functions along the dispersions $\omega = v|q_n|$, originating from each Bragg point, with intensity proportional to $Q^2e^{-2W}\,kT/\omega^2$. Anharmonic terms in the inter-

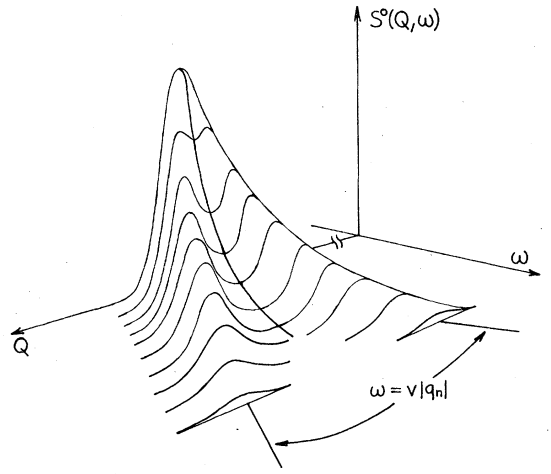

FIG. 3. Qualitative behavior of the independent-chain scattering function, Eq. (4), at a given sheet n, centered at $Q_n = n\,2\pi/d$. q_n is defined as $|q_n| = |Q - Q_n|$. Only the $\omega \geq 0$ part is shown.

atomic forces affect the Debye-Waller factor as well as the sharpness of the phonon excitations, which is usually accounted for by replacing the δ functions by Lorentzians of finite width.

The cross section, Eq. (4), differs in several ways from the above-mentioned behavior, especially in the small ω, q_n range. Being the product of two Lorentzians centered at $\omega = vq_n$ and $\omega = -vq_n$, respectively, the qualitative features of $S^0(Q,\omega)$ at a given sheet n are those shown in Fig. 3. Considered as a function of q_n, $S^0(Q,\omega)$ displays two nearly Lorentzian peaks with FWHM equal to $2k_n$, provided ω is sufficiently large. In the same limit, it is seen that each peak has an intensity proportional to $k_n/\omega^2 \propto Q^2\ T/\omega^2$. Apart from the missing Debye-Waller factor, this is in agreement with the one-phonon cross section. However, the finite width κ_n of the cross section [Eq. (4)] is a result of the lack of long-range order in the system, rather than anharmonic effects [the Hamiltonian H^0, Eq. (1) is purely harmonic]. κ_n is independent of ω, whereas the anharmonic line width to a first approximation is expected to increase with ω. For smaller values of ω the line shape of $S^0(Q,\omega)$ changes and at $\omega = 0$ it becomes a squared Lorentzian, and thus remains finite for $\omega = 0$. This means that the elastic scattering is infinitely small, there is no Bragg peak proportional to $\delta(\omega)$. It is thus predicted that the sheets of scattering from the Hg chains are of exclusively inelastic origin. The absence of Bragg peaks and Debye-Waller factor in Eq. (4) reflects the fact that the atoms of the chain described by the Hamiltonian Eq. (1) have no fixed equilibrium positions, as is the case for a liquid. Therefore, it is expected from the theoretical model, that the physical properties of the Hg chains in the high-temperature limit are those of a "one-dimensional liquid."

In an experimental test of the theoretical model, it is clear from the preceding discussion that one should specifically address the following questions: (i) Do the intrinsic widths $\kappa_n(T)$ of quasi-elastic scans through various sheets at various temperatures obey the relation given by Eq. (3)? (ii) Does $S^0(Q,\omega = 0)$ [given by Eq. (4)] exhaust all scattering cross sections at $\omega = 0$? (iii) Are inelastic scans through the sheets adequately interpreted in terms of the scattering function of Eq. (4), especially are the intrinsic widths of the "phonon peaks" given by Eq. (3) and thus independent of ω? As far as point (iii) goes, it would be desirable to do inelastic measurements at higher order ($n > 1$) sheets, however, due to intensity and absorption problems, we have been able to do inelastic scans only at the first ($n = 1$) sheet.

III. EXPERIMENT AND DATA ANALYSIS

The sample crystal used in the present investigation was the same as that used earlier.[11] All measurements were carried out on a triple-axis neutron spectrometer at the Brookhaven High-Flux Beam Reactor. The sample was mounted in a closed-cycle refrigerator capable of controlling the temperature to within 0.1 K in the range from 10–300 K. The orientation of the crystal was that indicated in Fig. 1a, i.e., with the $(h0l)$ zone in the scattering plane. Most scans were carried out using a fixed incoming neutron energy E_i and each point was counted for a fixed monitor value. Essentially two different kinds of scans were performed. For the inelastic scattering measured at the first ($n = 1$) sheet (Secs. IV B and C) E_i was equal to 5 or 14.7 meV and the horizontal collimation adjusted to meet the requirements of resolution in the individual cases. Pyrolytic graphite of mosaic spread to 24′, reflecting from (002) planes was used for monochromator and analyzer, and a cooled Be filter and a pyrolytic graphite filter was used to remove higher-order neutrons from the 5 and 14.7 meV beams, respectively.

As is well known, the experimentally observed scan profile results from a convolution of the scattering cross section of the sample crystal and the resolution function of the spectrometer. In the analysis of the data of the present investigation, we used a standard computer program capable of least-squares fitting a number of parameters specifying a given analytical shape of the cross section to the experimental scan profile by means of a numerical integration procedure. In

doing this, a constant background level of the scans was estimated in each case and no further corrections to the experimental points were carried out.

IV. EXPERIMENTAL RESULTS AND DISCUSSION

A. T and Q dependence of sheet widths

In order to test the predicted relation in Eq. (3) between the width parameter κ_n of the nth sheet, the temperature T and the order of the sheet n, we carried out the following two series of scans: (i) Constant E scans with $\Delta E = 0$ were performed with $\vec{Q} = \zeta a_L^*$, scanning across the third ($n = 3$) sheet at different temperatures ranging from 120–300 K. Pyrolytic graphite was used as monochromator and analyzer [(004) and (002) reflections, respectively] and the horizontal collimation was 10′-20′-10′-40′. (ii) At $T = 295$ K scans with $\vec{Q} = \zeta a_L^*$, across the sheets from $n = 1$ to $n = 7$ were carried out. The spectrometer configuration for $n = 1, 2, 3$ was identical to the above mentioned. For $n = 5, 6, 7$, we used $E_i = 180$ meV and a Be (110) monochromator. No analyzer was used here and the collimation was 10′-20′-10′.

The experimental peaks obtained from the scans specified above were analyzed by means of the independent-chain cross section, Eq. (4). In all the fittings v was kept constant and equal to $v = 23.8$ meV Å as found from the inelastic measurements presented in Sec. IV B. From the first series of scans, we thus determined the value of κ_3 as a function of temperature, and the results are shown in Fig. 4. Likewise, Fig. 5 shows the fitted value of κ_n at room temperature as a function of n^2, as found from the second series of scans. The straight lines in Figs. 4 and 5 represent the predicted relation, Eq. (3), between κ_3 and T and between κ_n and n^2, respectively, using the values $v = 23.8$ meV Å and $d = 2.655$ Å. It is seen from Figs. 4 and 5 that the experimentally determined behavior of κ_n conforms to the n^2T dependence expected for harmonic one-dimensional chains. The experimental magnitudes of κ_n fall uniformly ~20% below the theoretical values, $\kappa_n = 2\pi^2 kTn^2/mv^2d$, if we use $v = 23.8(1.0)$ meV Å as found in Sec. IV B. It is not clear how seriously to take this discrepancy. Before more esoteric explanations are sought, it might be well to confirm, (a) the precise degree to which v is independent of momentum components perpendicular to the chain direction and (b) the absence of significant nonlinear dispersion along the chain direction, produced for example by longer than nearest-neighbor forces. [The width κ_n is due to phonon fluctuations with energy up to ~k_BT. Thus the v appearing in Eq. (3) should represent an average over a phonon

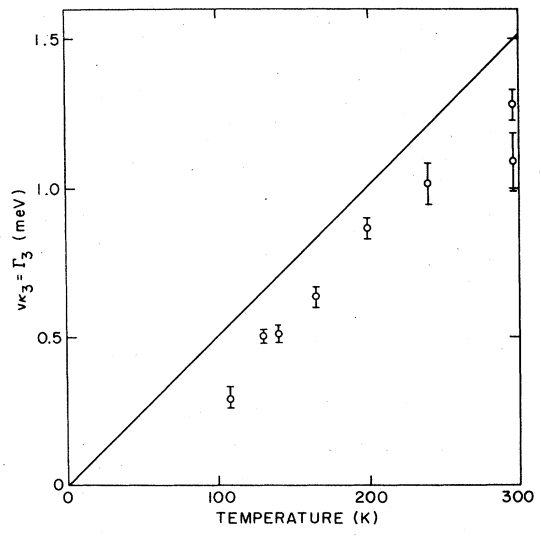

FIG. 4. Values of the width parameter $v\kappa_3 = \Gamma_3$ as found from fitting the cross section [Eq. (4)] to $\Delta E = 0$ scans through the third sheet at various temperatures. The value of v used was $v = 23.8$ meVÅ found from the room temperature scans shown in Fig. 6. The straight line shows the theoretical predicted relation between $v\kappa_3$ and T [Eq. (3)] inserting $v = 23.8$ meVÅ and $d = 2.655$ Å.

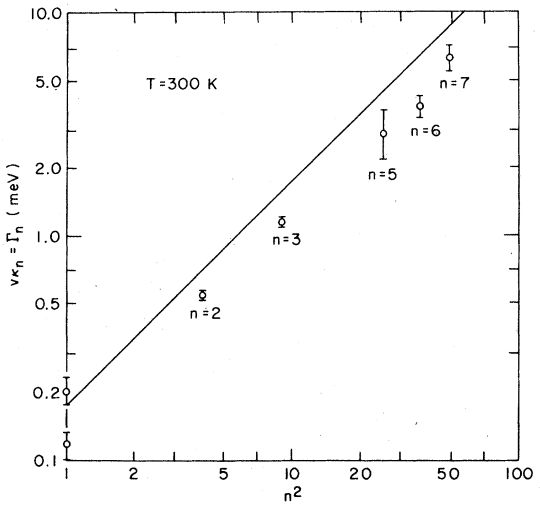

FIG. 5. Values of the width parameter $v\kappa_n = \Gamma_n$ as found from fitting the cross section [Eq. (4)] to $\Delta E = 0$ scans through sheets $n = 1$ to $n = 7$ at room temperature. The value of v was made equal to $v = 23.8$ meVÅ. The straight line shows the theoretically predicted relation between $v\kappa_n$ and n^2 [Eq. (3)] for $T = 300$ K, inserting $v = 23.8$ meVÅ and $d = 2.655$ Å. The point for $n = 4$ was omitted because of a disturbing Al-powder peak from the sample dewar at this value of momentum transfer.

energy range of ~25 meV at room temperature, much greater than the 2-meV range studied here.]

B. Inelastic measurements at the first sheet at room temperature

A series of constant E scans was carried out at room temperature along the a_L^* direction ($\vec{Q} = \zeta a_L^*$), scanning across the position of the first ($n = 1$) sheet at $Q_1 = 2.83\ a_L^*$. The range of energy transfer ΔE was 0–1.75 meV. The use of the constant E mode rather than the constant Q mode was motivated by the steep dispersion relation of the Hg chain excitations previously observed.[3] Some representative scans are shown in Fig. 6. The different symbols of the experimental points refer to different spectrometer configurations as described in the figure caption. The solid curves show the result of least-squares fits to the experimental scans as described in Sec. III, using the independent-chain cross section [Eq. (4)]. For each scan, the fitting involves three adjustable parameters: an intensity scale factor A, the sound velocity v and the width parameter κ_1. In all but one scan ($\Delta E = 0.0$) all three parameters were least-squares fitted independently. The last three columns of Table I show the values and standard deviations of A, v and κ_1 thus found. The weighted average value of v from the scans of ΔE between 0.2 and 1.7 meV is found to be

$$\sum \frac{v_i}{\sigma_i} \Big/ \sum \frac{1}{\sigma_i} = 23.8(1.0)\ \text{meV Å},$$

where the uncertainty is estimated from the spread in individual values of v. Due to a high correlation between v and κ_1 in the fitting of the $\Delta E = 0$ scan, the value of v was here kept fixed and equal to the average value of 23.8 meV Å. In each group of

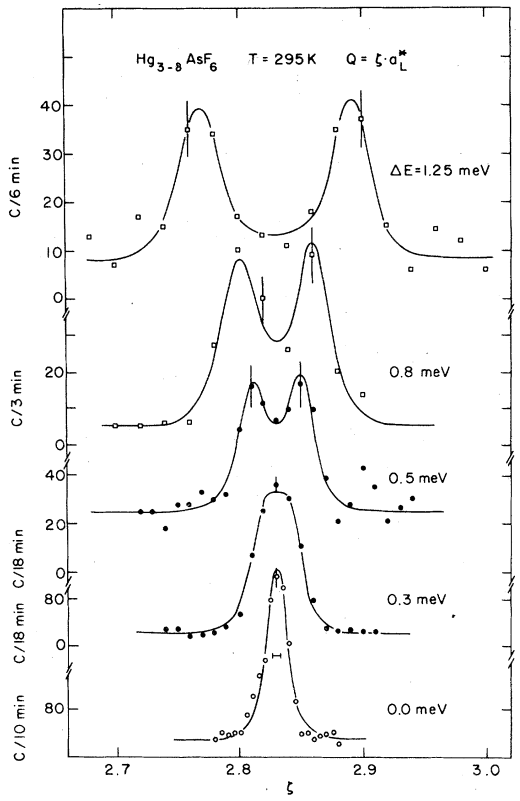

FIG. 6. Constant E scans at $T = 295$ K performed along the a_L^* direction ($\vec{Q} = \zeta a_L^*$) covering the first ($n = 1$) sheet at $\zeta = 2.83$. The spectrometer configurations were the following: open circles: $E_i = 5$ meV, 20′-20′-20′-40′; filled circles: $E_i = 5$ meV, 40′-40′-40′-40′; squares: $E_i = 14.7$ meV, 20′-20′-20′-20′. ΔE denotes the energy transfer. Solid curves are computer fits using the cross section (4), the parameters of which thus found are listed in Table I. The horizontal bar in the $\Delta E = 0$ scan indicates the full width at half-maximum of a $\delta(\Delta E)$ component in the cross section.

TABLE I. Values of intensity scale factor A, sound velocity v and width parameter κ_1 found from fitting the cross section (4) to constant E scans through the first sheet, at room temperature. The spectrometer configurations of the individual scans are specified by either the fixed incoming neutron energy (E_i) or the fixed outgoing neutron energy (E_f) and the horizontal collimations (coll.).

		Spectrometer configurations					
Scan no.	ΔE(meV)	E_i(meV)	E_f(meV)	Coll. (′)	A	V(meVÅ)	κ_1(Å^{-1})
1	0	5	•••	20-20-20-40	21(2)	23.8	0.0107(9)
2	0.2	•••	•••	•••	11(4)	25(6)	0.0096(30)
3	0.3	5	•••	40-40-40-40	7.9(0.4)	23(1)	0.0089(14)
4	0.5	•••	•••	•••	6.7(1.0)	25(1)	0.0083(18)
5	0.7	14.7	•••	20-20-20-40	14(3)	23(1)	0.0070(20)
6	0.8	•••	•••	•••	20(10)	26(1)	0.0061(15)
7	1.15	•••	•••	•••	18(2)	25(1)	0.0035(17)
8	1.25	•••	•••	•••	29(7)	23(1)	0.0073(19)
9	1.75	•••	•••	•••	13(5)	25(2)	0.0110(5)
10	0	•••	14.7	40-20-40-40	7.2(0.2)	22.0	0.0060(5)
11	1.5	•••	•••	•••	5.5(1.2)	22(2)	0.0072(30)

identical spectrometer configurations, the scans have been scaled to a common value of the monitor counts.

One notices from Table I that most of the fitted values of A, v and κ_1 display quite large relative uncertainties. If we focus our attention to the κ_1 column, it is seen that all values are within two standard deviations of the average value $\langle\kappa_1\rangle = 0.0075(20)$ Å^{-1}. The theoretically predicted relation Eq. (3) between κ_n and v can now readily be tested for $n = 1$. Inserting in Eq. (3) $v = 23.8$ (1.0) meV Å gives $\kappa_1 = 0.007(1)$ meV Å, which agrees well with the mean value $\langle\kappa_1\rangle$ found from the experimental curves. We thus see that the fitted widths of the inelastic scans at the first ($n = 1$) sheet although scattered, show no systematic dependence on energy transfer, in accordance with the theoretical prediction in Eq. (3).

Besides the values of v and κ_1 and their interrelation, the fitted values of the intensity scale factor A (column 6 in Table I) provide a test of the model predictions. Specifically, we expect that within each group of a given spectrometer configuration, the scans should give the same value of A. This condition is moderately well fulfilled for most of the scans (Nos. 3 and 4 and Nos. 5–9). However, the $\Delta E = 0$ scans (Nos. 1 and 10) have somewhat larger A values than their $\Delta E \neq 0$ counterparts. In order to test these scans more carefully for the presence of a truly elastic component, they were refit allowing for an adjustable contribution of the form $B\delta(\omega)\delta(q_n)$. Negligible values of B resulted. We therefore conclude that the cross section contains no elastic component and consider the weak indication of excess $E = 0$ cross section as unexplained and possibly spurious. With this proviso, the theoretical cross section, Eq. (4), provides a very satisfactory description of the observed scan profiles on the first sheet.

C. Measurements at the first sheet at various temperatures

Figure 7 shows the peak values of the cross section, Eq. (4), fitted to the constant E scans through the first sheet at room temperature, as found in the previous section. As was discussed in detail, all scans were adequately interpreted in terms of the independent-chain Hamiltonian, Eq. (1), thus demonstrating the purely one-dimensional behavior of the Hg chains. Particularly, the dispersion of the Hg chain excitations goes to zero at $Q = Q_1$ (to within the instrumental resolution limit), as indicated in Fig. 7.

Interaction forces along the chain direction between the host lattice and the Hg chains (such as, e.g., pinning or impurity effects) as well as interactions between the individual Hg chains will in general modulate the pure one-dimensional dispersion of the Hg chain excitations, as found at room temperature (Fig. 7). In particular, one expects these interactions to create an energy gap. In order to investigate such effects, inelastic scans through the first sheet similar to those presented in the previous section were carried out at several temperatures below 295 K. Special attention was paid to the details of the dispersion around $\vec{Q} = (Q_1, 0, 0)$ and high instrumental resolution was obtained by using $E_i = 5$ meV and horizontal collimation equal to 20′-10′-20′-20′. It is found that a small, but well-defined energy gap Δ at $\vec{Q} = (Q_1, 0, 0)$, as sketched in Fig. 2, develops at temperatures below T_c.[11] The gap most clearly manifests itself in constant Q scans performed at $\vec{Q} = (Q_1, 0, 0)$ as that shown in Fig. 8(a), taken at $T = 70$ K. For comparison, an identical scan, taken at $T = 150$ K, is shown in Fig. 8(b).

Besides the scan shown in Fig. 8(a), a series of constant E scans similar to those shown in Fig. 6 was performed at $T = 70$ K. All scans taken below T_c were computer fitted using a damped harmonic-oscillator cross section with the dispersion

$$\hbar\omega = (\Delta^2 + v^2 q_1^2)^{1/2}. \qquad (5)$$

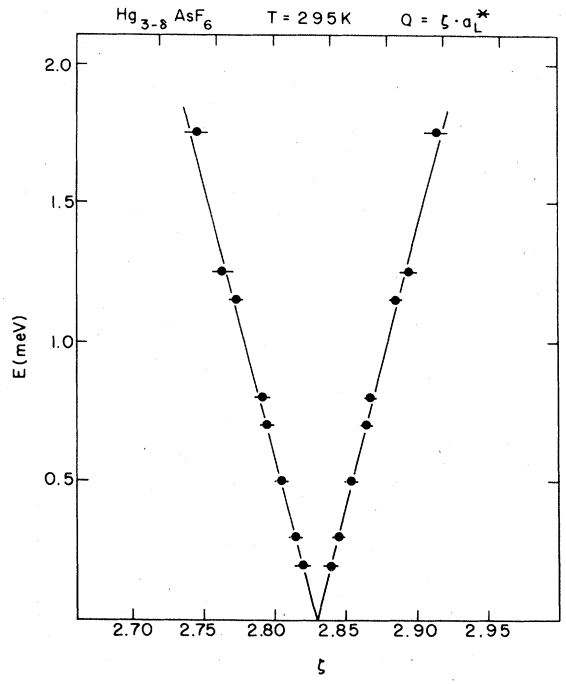

FIG. 7. Peak values of the cross section (4) fitted to constant E scans through the first sheet at room temperature. The straight lines are drawn with the slope $v = 23.8$ meVÅ found as the average value of v's fitted to the individual scans.

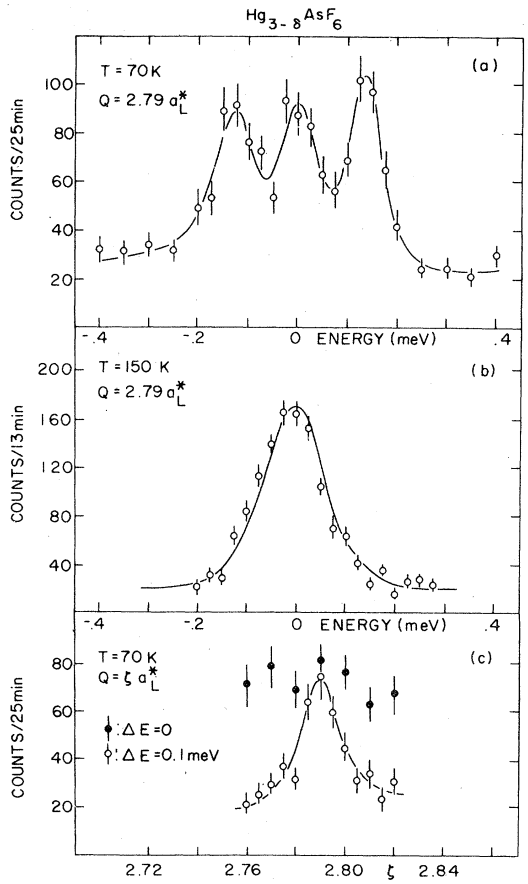

FIG. 8. (a) Constant Q scan at 70 K for $\vec{Q} = 2.79\vec{a}_L^*$ (= sheet position at T = 70 K) showing the energy gap in the Hg chain dispersion. The curve is a guide to the eye only. (b) Constant Q scan at 150 K for $\vec{Q} = 2.79\vec{a}_L^*$. The curve shows a fit to the experimental points using the cross section (4). (c) Constant E scans at 70 K for $\Delta E = 0$ (solid circles) and for $\Delta E = 0.1$ meV (open circles), showing the incoherency of the peak at $\Delta E = 0$ in (a). The curve is a guide to the eye only.

In the fitting of the constant Q scans at $\vec{Q} = (Q_1, 0, 0)$, v was kept fixed and equal to the room temperature value 23.8 meVA. The value of Δ thus found was kept fixed in the fittings of the constant E scans, thus giving values of v. The energy gap Δ found from fittings to constant Q scans at various temperatures is shown in Fig. 1(b) (open circles). The peak values of the cross section found from the analysis of the 70 K scans are shown in Fig. 9 (left part). The solid curve shows the dispersion relation Eq. (5) with $\Delta(70\text{ K}) = 0.10(1)$ meV and $v = \langle v(70\text{ K})\rangle = 29(1)$ meV Å found as the average value from the individual scans. (It was checked that the determination of Δ from the constant Q scan was quite insensitive to the fixed value of v used in the fitting.)

There are several aspects of the data presented above which should be examined closely. One notes from Fig. 1(b) that $\Delta(T)$ displays the qualitative behavior of an order parameter [the Bragg intensity developing below T_c, also shown in Fig. 1(b)] and expecially that Δ is very small (<0.01 meV) if not zero above T_c. From this we may readily conclude that it is the interchain coupling (responsible for the phase transition) which causes the presence of Δ, and the excitation at the gap can (in the low-temperature limit) be considered as a normal mode of the Hg ion sublattice. As mentioned in the introduction, it was established in a previous neutron study[10] that at temperatures below T_c the Hg ions form a regular sublattice with reciprocal lattice points at $[h(3\text{-}\delta),\ k \pm h\delta, l]$, $h + k + l = 2n$ for the array of chains parallel to a_L and at $[h \pm k\delta, k(3\text{-}\delta), l]$, $h + k + l = 2n$, for the array of chains parallel to b_L. The plus-and-minus signs reflect the formation of two equivalent domains. A portion of the points $[h(3\text{-}\delta), k + h\delta, l]$ $h + k + l = 2n$, is shown in Fig. 9 (right part). The point (3-δ, 0, 0) (denoted by A) of observation of the gap is seen to be close to a zone-boundary point (for both domains). Therefore, the eigenvector of the mode observed at the gap is close to that of an out-of-phase vibration of neighboring parallel chains with displacements along the chain

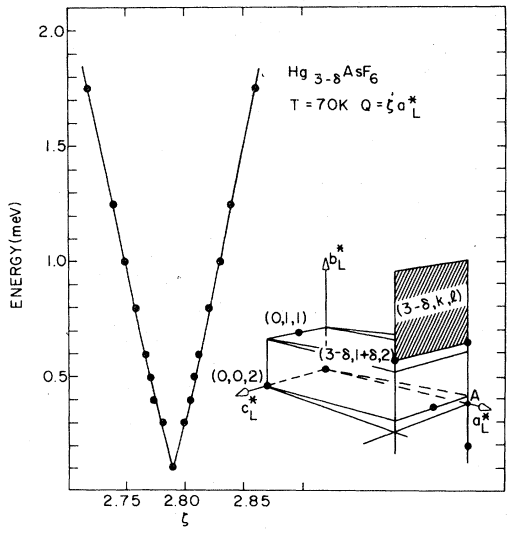

FIG. 9. Left-hand side shows peak values of a damped harmonic oscillator cross section with the dispersion of Eq. (5), fitted to constant E scans across the first sheet, taken at 70 K. The curve shows the dispersion (5) with $\Delta = 0.103$ meV and $v = 29$ meVÅ. The right-hand side shows reciprocal lattice points of the phase-ordered array of Hg-chains along the a_L direction. The hatched plane indicates the first diffuse sheet and A ($= 2.79\vec{a}_L^*$) is the point of observation of the gap.

direction. Consequently, the value of Δ relates directly to the shear force constant between parallel chains. Going from A in the c_L^* direction, one approaches the Bragg points $(3-\delta, \pm\delta, 1)$ (without reaching them), and the dispersion in this direction is thus expected to decrease smoothly, as indicated in Fig. 2. This behavior, however, remains to be verified by experiment.

The presence of the gap makes it straightforward to demonstrate that there is no elastic scattering associated with the "sheet" in the ordered phase below T_c. This is shown by the two constant E scans plotted in Fig. 8(c). The closed circles correspond to $\Delta E = 0$ and are seen to be independent of Q, while the open circles correspond to $\Delta E = 0.1$ meV and thus scans through the lowest part of the cross section. Thus, the peak at $\Delta E = 0$ observed in the scan of Fig. 8(a) is entirely incoherent. Considering that the high-temperature phase, as opposed to the low-temperature phase, is characterized by the lack of correlations between different Hg chains, the observation of absence of elastic scattering observed at $\vec{Q} = (3-\delta)\vec{a}_L^*$ below T_c strongly supports the similar, albeit less clear cut conclusion, we arrived at for the room-temperature case (Sec. IV B).

Finally, we notice from the low-temperature data, that at $T = 70$ K, the slope of the Hg chain dispersion $\langle v(70\text{ K})\rangle = 29(1)$ meV Å is ~20% larger than at room temperature. The physical reason for this substantial stiffening of the Hg chains at lower temperatures is not clear to us, but it might be related to the freezing of the chains into an ordered sublattice below T_c. Obviously, the purely harmonic independent-chain Hamiltonian (1) cannot account for the observed effect, and it would therefore be desirable to have a set of inelastic scans in the high-temperature regime, besides that at $T = 295$ K, in order to further test the validity of the harmonic approximation in Eq. (1).

D. Acoustic lattice phonons at room temperature

Figure 10 shows results obtained at room temperature from constant Q scans of acoustic lattice phonons in the $\Delta(\zeta 00)$ and $\Lambda(00\zeta)$ directions. Scans were carried out for $\vec{Q} = (2+\zeta, 0, 0)$ and $(\zeta, 0, 4)$ thus measuring respectively LA- and TA-modes propagating along Δ, with the TA modes polarized along Λ. Likewise, for $\vec{Q} = (0, 0, 8+\zeta)$ and $(2, 0, -\zeta)$, LA- and TA-modes propagating along Λ were measured, respectively, with the TA-modes polarized along Δ. The incoming neutron energy E_i and horizontal collimation used was 5 meV and 40′-40′-40′-40′, respectively, apart from the scans in the vicinity of (008), where

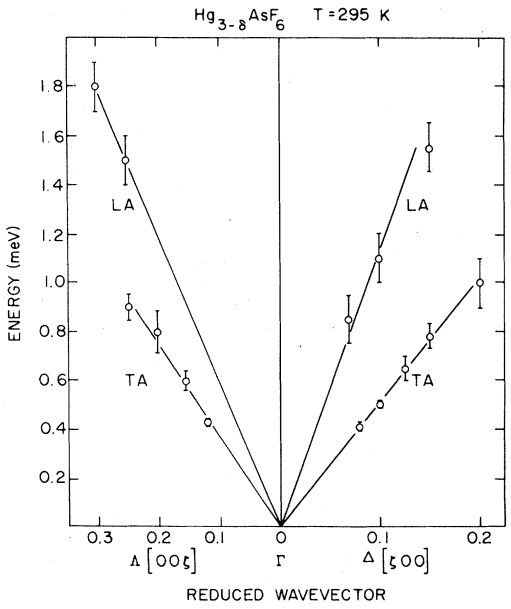

FIG. 10. Peak values of constant Q scans showing acoustic phonons in the $\Lambda(00\zeta)$ and the $\Delta(\zeta 00)$ directions. The measurements were carried out at room temperature.

$E_i = 14.7$ meV and collimation 20′-20′-20′-40′ was applied. With the resolution thus obtained phonon groups could be measured for wave numbers down to $|\vec{q}| \sim 0.06$ Å^{-1}.

It is seen from Fig. 10 that the acoustic dispersions in the observable $\vec{q}$ range are approximately linear, and we can immediately determine the slopes. The results yield

$$V(\text{TA}, \Delta) = 6.00 \pm 0.25 \text{ meVÅ} = 912 \pm 35 \text{ m/sec},$$

$$V(\text{TA}, \Lambda) = 7.50 \pm 0.50 \text{ meVÅ} = 1140 \pm 75 \text{ m/sec},$$

$$V(\text{LA}, \Delta) = 14.0 \pm 2 \text{ meVÅ} = 2130 \pm 300 \text{ m/sec},$$

$$V(\text{LA}, \Lambda) = 12.0 \pm 1 \text{ meVÅ} = 1800 \pm 150 \text{ m/sec}.$$

It is known from linear elasticity theory[14] that for tetragonal lattices $C_{44} = C_{55}$ and thus elastic transverse modes along z polarized along x are expected to have the same velocity as the elastic transverse modes along x polarized z, both given by $v = (C_{44}/\rho)^{1/2}$. Thus the measured slopes of the transverse acoustic branches stated above seem to violate the elastic symmetry requirement.

We believe that the failure of the measured phonon dispersion to conform to the predictions of elastic theory can be traced to the extreme anisotropy of elastic forces resulting from the incommensurate nature of $Hg_{3-\delta}AsF_6$. There is as yet no theory of the long-wavelength lattice dynamics of interpenetrating incommensurate

sublattices which adequately addresses surface and pinning forces. We outline below a simple theory of the long-wavelength behavior of a *commensurate*, but anisotropic two-sublattice model, which contains some essential features of an incommensurate model. The results help to clarify the nature of the anomalous behavior observed in these experiments and suggest the importance of further investigations of the elastic behavior of materials of this type.

It is well known[15] that long-wavelength lattice dynamics can be discussed quite generally by an expansion of the dynamical matrix

$$D^{kk'}_{\alpha\beta}(\vec{q}) = (m_k m_{k'})^{-1/2} \times \left\{ \Phi^{(0)}(k,k')_{\alpha\beta} + q^2 \sum_{\gamma\lambda} \Phi^{(2)}(k,k')_{\alpha\beta,\gamma\lambda} \hat{q}_\gamma \hat{q}_\lambda + \cdots \right\} . \quad (6)$$

Here m_k is the atomic mass of the kth sublattice, $\hat{q}$ is a unit vector along $\vec{q}$ (i.e., $\vec{q} = |q|\hat{q}$) and all Greek subscripts represent Cartesian components (x,y,z). We have specialized to the inversion symmetric case thereby eliminating terms linear in q. For simplicity we further specialize to a crystal system, (i) with orthorhombic or higher symmetry (so that the principal axes of second-rank tensor quantities are Cartesian) (ii) interacting through central forces only, and (iii) with two sublattices, $(k,k') = (A,B)$. The components of $\Phi^{(0)}$ and $\Phi^{(2)}$ can be written in the form

$$\Phi^{(0)}(k,k')_{\alpha\beta} = \mu\Omega^2_\alpha \delta_{\alpha\beta}(2\delta_{k,k'} - 1) ,$$
$$\Phi^{(2)}(k,k')_{\alpha\beta,\gamma\lambda} = \delta_{\alpha\beta}\delta_{\gamma\lambda}\eta^{k,k'}_{\gamma\lambda} + c^{k,k'}_{\alpha\beta,\gamma\lambda} , \quad (7)$$

where $\mu = m_A m_B/(m_A + m_B)$ is the reduced mass and Ω_α is the $\vec{q} = 0$ mode frequency of the coupled lattice for a mode with polarization along α. For $k \neq k'$, $\eta^{k,k'}_{\gamma\gamma}$ can be thought of as the stress acting on sublattice k due to the presence of sublattice k'. Elements of $\eta^{k,k'}_{\gamma\lambda}$ diagonal in k are given by requiring zero net stress, $\sum_{k,k'} \eta^{k,k'}_{\gamma\gamma} = 0$. The $c^{k,k'}_{\alpha\beta,\gamma\lambda}$ display the same symmetry properties as the macroscopic elastic constants and in particular they are unchanged by the permutations $(\alpha\beta) \rightarrow (\beta\alpha)$, $(\gamma\lambda) \rightarrow (\lambda\gamma)$ and $(\alpha\beta,\gamma\lambda) \rightarrow (\gamma\lambda,\alpha\beta)$. Using these relations we may discuss the long-wavelength behavior of the coupled system for any propagation direction, $\vec{q}$. For the present purpose it is sufficient to discuss modes propagating along a symmetry axis, $\hat{q} = \hat{q}_\gamma$. The dynamical matrix is then diagonal in Cartesian indices and the transverse modes $(\alpha \neq \gamma)$ are obtained by diagonalizing a 2×2 matrix with elements

$$D^{k,k'}_{\alpha\alpha}(\vec{q}_\gamma) = \mu\Omega^2_\alpha(2\delta_{k,k'} - 1)(m_k m_{k'})^{-1/2} + \lambda^{k,k'}_{\alpha\alpha,\gamma\gamma} q^2_\gamma , \quad (8)$$

where

$$\lambda^{k,k'}_{\alpha\alpha,\gamma\gamma} = (\eta^{k,k'}_{\gamma\gamma} + c^{k,k'}_{\alpha\alpha,\gamma\gamma})(m_k m_{k'})^{-1/2}$$

The behavior of the solutions of Eq. (8) depend upon the value of q_γ compared to a natural inverse length ξ_γ which can be defined by

$$\Omega^4_\alpha = [(\lambda^{AA}_{\alpha\alpha,\gamma\gamma} - \lambda^{BB}_{\alpha\alpha,\gamma\gamma})^2 + (2\lambda^{AB}_{\alpha\alpha,\gamma\gamma})^2]\xi^4_\gamma .$$

(i) The small q or coupled limit, $q_\gamma \ll \xi_\gamma$. The two sublattices are tightly coupled and the modes polarized along α consist of an optic mode with $\omega^2 = \Omega^2_\alpha$ + terms of order q^2_γ, and an acoustic mode with

$$\left(\frac{\omega}{q_\gamma}\right)^2 = (m_A + m_B)^{-1} \sum_{k,k'} c^{k,k'}_{\alpha\alpha,\gamma\gamma} ,$$

which is symmetric in (α,γ) in accord with elastic theory.

(ii) The large q or uncoupled limit, $q_\gamma \gg \xi_\gamma$. Both eigenvectors are those of acoustic modes propagating independently in their respective sublattices. The dispersion is also linear with

$$(\omega_\pm/q_\gamma)^2 = \tfrac{1}{2}[(\lambda^{AA}_{\alpha\alpha,\gamma\gamma} + \lambda^{BB}_{\alpha\alpha,\gamma\gamma}) \pm (\Omega_\alpha/\xi_\gamma)^2] .$$

In most normal materials, ξ_γ is sufficiently large that the coupled limit (i), is adequate over the entire q range for which long-wave elastic theory is valid. Only in the case of exceptionally small Ω_α can one find also the other behavior. For these ideas to apply to a material composed of interpenetrating incommensurate chains, the model must have a pronounced anisotropy. Specifically, it is to be expected that the forces coupling the two sublattices are weak (in principle, nonexistent, except for surface and impurity pinning effects) for relative displacements along the chain direction, but of normal strength for displacements perpendicular to the chain. If x and z are chosen to lie respectively parallel and perpendicular to the chain direction, we expect $\Omega_z \gg \Omega_x \approx 0$. Therefore $\xi_z \gg \xi_x \approx 0$, which implies that even the smallest wave vectors $q = q_z$ probed by neutrons may fall within the large q uncoupled regime, whereas all wave vectors $q = q_x$ are in the normal, coupled, regime. Such a set of anisotropic dispersion relations is shown schematically in Fig. 11 for both transverse modes (upper part) and longitudinal modes (lower part), which may be similarly analyzed. It is clear that under such conditions one may expect the effective elastic constants derived from sound velocities to be symmetric second rank tensors only if $q_\gamma \ll \xi_\gamma$ even for γ along the chain direction. It would be of considerable interest to investigate this aspect

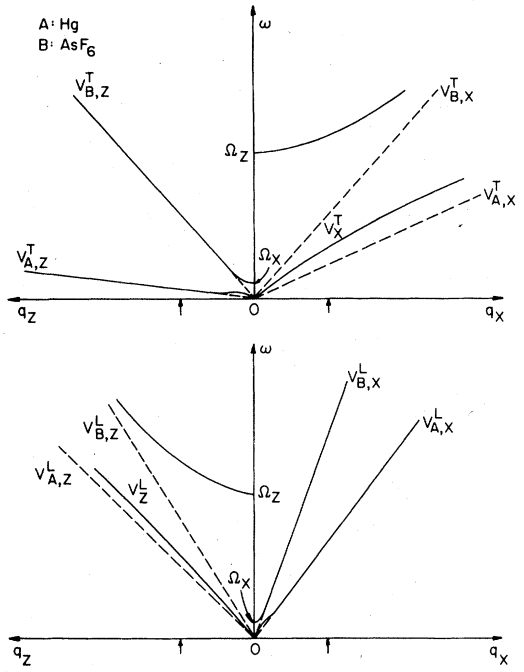

FIG. 11. Schematic illustration of phonon dispersion relations in a highly anisotropic two-sublattice system. The upper part shows transverse branches, those along x polarized along z and vice versa. The lower part shows longitudinal modes. The intersublattice force constants of shear displacements along x are assumed much smaller than those along z, thus imitating the chain-structural feature of $Hg_{3-\delta}AsF_6$ [x corresponds to a a_L (or b_L) and z corresponds to c_L]. The small arrows at the q axis serve to indicate the lower limit of inelastic neutron measurements. $V^{T(L)}_{k,\alpha}$ denotes the transverse (longitudinal) sound velocity propagating along α of the uncoupled sublattice k (dashed lines).

of the elastic behavior of $Hg_{3-\delta}$ AsF_6 at much lower hyper and ultrasonic frequencies in order to attempt to determine $\xi_x = \xi_y$ in this material. This is particularly so because the ξ_x are closely related to the $q = 0$ gap frequencies Ω_γ concerning which, there is at present, much uncertainty.

V. SUMMARY AND CONCLUSIONS

In summary, we have studied by means of quasielastic and inelastic neutron scattering the dynamical properties of $Hg_{3-\delta}$ AsF_6. Special attention has been paid to the physics of the Hg chains. At temperatures well above $T_c = 120$ K we have shown that the scattering function from the chains reflects liquid-like behavior and is in quantitative agreement with theoretical predictions by Emery and Axe. In particular, the chains have no long-range order and give rise to entirely inelastic scattering. Furthermore, for temperatures above T_c the one-dimensional dispersion of phononlike excitations in the chains, emerging from the sheets, goes to zero at the sheet positions. These observations are manifestations of the incommensurate nature of the system as well as the fact that pinning of the chains to impurities or other imperfections plays a minor role. Thus, we have demonstrated that well above T_c, the chains of Hg ions in $Hg_{3-\delta}$ AsF_6 constitute a unique realization of a one-dimensional liquid.

Below T_c, the "Hg liquid" freezes into a three-dimensional long-range ordered, though still incommensurate substructure within the AsF_6 sublattice. A small (~0.1 meV) energy gap develops in the Hg chain dispersion, arising from the interaction between different chains. The excitation at the energy gap can be considered as a shear mode in the Hg ion sublattice, with a wave vector close to the zone boundary and perpendicular to the chains. The value of the energy gap thus relates to the shear force constant between neighboring chains, and goes to zero at $T = T_c$. The response of this low-lying excitation remains well defined and underdamped to energies below ~0.07 meV, and contains no elastic component. These observations indicate that below T_c the system of Hg ions is remarkably "perfect," with anharmonic and pinning effects playing a minor role.

Finally, we have measured at room temperature some acoustic phonon branches of the lattice, showing an apparent failure of transverse modes along c_L and a_L to conform to predictions of elasticity theory. We have shown by means of a simple (commensurate) two-sublattice dynamical model that this type of behavior can be expected in systems with extreme anisotropy in the force constants coupling the two sublattices. Applied to the case of $Hg_{3-\delta}$ AsF_6 the model predicts for the acoustic transverse branches an elastic regime along the c_L axis anomalously small (compared to the "normal" behavior along the a_L axis), and thus impossible to probe with neutrons. It is unlikely, however, that the model can be carried through to a quantitative stage, since it is necessarily based on commensurability. It would be desirable to supplement the present neutron results with ultrasonic measurements.

ACKNOWLEDGMENTS

The authors are indebted to V. J. Emery and R. Currat for stimulating discussions on the subject. Research at Brookhaven was supported by the Division of Basic Energy Sciences, Department of Energy, under Contract No. EY-76-C-02-0016. Research at the University of Pennsylvania was supported by the NSF-MRL Program (DMR 76-00678).

*Present address: Dept. of Physics, University of Pennsylvania, Philadelphia, Pa. 19104
†Present address: Dept. of Chemistry, University of Pennsylvania, Philadelphia, Pa. 19104

[1]I. D. Brown, B. D. Cutforth, C. G. Davies, R. J. Gillespie, P. R. Ireland, and J. E. Vebries, Can. J. Chem. 52, 791 (1974).
[2]A. J. Schultz, J. M. Williams, N. D. Miro, A. G. MacDiarmid, and A. J. Heeger, Inorg. Chem. 17, 646 (1978).
[3]J. M. Hastings, J. P. Pouget, G. Shirane, A. J. Heeger, N. D. Miro, and A. G. MacDiarmid, Phys. Rev. Lett. 39, 23, 1484 (1977).
[4]T. Wei, A. F. Garito, C. K. Chiang, and N. D. Miro, Phys. Rev. B 16, 3373 (1977); R. Spal, C. K. Chiang, A. Denenstein, A. J. Heeger, N. D. Miro, and A. G. MacDiarmid, Phys. Rev. Lett. 39, 650 (1977); C. K. Chiang, R. Spal, A. Denenstein, A. J. Heeger, N. D. Miro, and A. G. MacDiarmid, Solid State Commun. 22, 293 (1977); E. Ehrenfreund, P. R. Newman, A. J. Heeger, N. D. Miro, and A. G. MacDiarmid, Phys. Rev. B 16, 1781 (1977); C. K. Chiang, M. J. Cohen, A. J. Heeger, N. D. Miro, and A. G. MacDiarmid, *ibid.* B 15, 4607 (1977).
[5]A. J. Heeger and A. G. MacDiarmid, Ann. N.Y. Acad. Sci. 313, 800 (1978); N. D. Miro, A. G. MacDiarmid, A. J. Heeger, A. F. Garito, C. K. Chiang, A. J. Schultz, and J. M. Williams, J. Inorg. Nucl. Chem. 40, 1351 (1978); D. P. Chakraborty, R. Spal, C. K. Chiang, A. M. Denenstein, A. J. Heeger, and A. G. MacDiarmid, Solid State Commun. 27, 849 (1978); E. Ehrenfreund, J. Kaufer, A. J. Heeger, N. D. Miro, and A. G. MacDiarmid, Phys. Rev. B 17, 4181 (1978).
[6]E. S. Koteles, W. R. Datars, B. D. Cutforth, and R. J. Gillespie, Solid State Commun. 20, 1129 (1976); B. D. Cutforth, W. R. Datars, A. van Schyndel, and R. J. Gillespie, Solid State Commun. 21, 377 (1977); G. A. Scholz, W. R. Datars, D. Chartier, and R. J. Gillespie, Phys. Rev. B 16, 4109 (1977); W. R. Datars, A. van Schyndel, J. S. Lass, D. Chartier, and R. J. Gillespie, Phys. Rev. Lett. 18, 40 (1978).
[7]R. Comès, G. Shirane, S. M. Shapiro, A. F. Garito, and A. J. Heeger, Phys. Rev. B 14, 6 (1976).
[8]V. J. Emery and J. D. Axe, Phys. Rev. Lett. 40, 23, 1507 (1978).
[9]J. D. Axe, *Solitions and Condensed Matter Physics*, edited by A. R. Bishop and T. Schneider (Springer-Verlag, Berlin, 1978), p. 234ff.
[10]J. P. Pouget, G. Shirane, J. M. Hastings, A. J. Heeger, and A. G. MacDiarmid, Phys. Rev. B 18, 7, 3645, (1978).
[11]I. U. Heilmann, J. M. Hastings, G. Shirane, A. J. Heeger, and A. G. MacDiarmid, Solid State Commun. 29, 469 (1979).
[12]R. B. Meyer and T. C. Lubensky, Phys. Rev. A 14, 2307 (1976).
[13]J. Als-Nielsen, R. J. Birgeneau, M. Kaplan, J. D. Litster, and C. R. Safinya, Phys. Rev. Lett. 39, 26, 1668 (1977).
[14]See, e.g., J. F. Nye, *Physical Properties of Crystals* (Oxford, Clarendon Press, 1957).
[15]M. Born and K. Huang, *Dynamical Theory of Crystal Lattices* (Oxford, Clarendon Press, 1954), p. 229ff.